Available online at www.sciencedirect.com
SCIENCE DIRECT®
C. R. Physique 5 (2004) 735–751
COMPTES RENDUS PHYSIQUE
http://france.elsevier.com/direct/COMREN/

Ice: from dislocations to icy satellites/La glace : des dislocations aux satellites de glace

Scale properties of sea ice deformation and fracturing

Jérôme Weiss [a,*], David Marsan [b]

[a] *Laboratoire de glaciologie et géophysique de l'environnement, UMR CNRS 5183, 54, rue Molière, BP 96, 38402 St Martin d'Hères cedex, France*
[b] *Laboratoire de géophysique interne et tectonophysique, UMR C5559, université de Savoie, campus scientifique, 73376 Le Bourget du Lac cedex, France*

Presented by Guy Laval

Abstract

The sea ice cover, which insulates the ocean from the atmosphere, plays a fundamental role in the Earth's climate system. This cover deforms and fractures under the action of winds, ocean currents and thermal stresses. Along with thermodynamics, this deformation and fracturing largely controls the amount of open water within the ice cover and the distribution of ice thickness, two parameters of high climatic importance, especially during fall and winter (no melting). Here we present a scaling analysis of sea ice deformation and fracturing that allows us to characterize the heterogeneity of fracture patterns and of deformation fields, as well as the intermittency of stress records. We discuss the consequences of these scaling properties, particularly for sea ice modelling in global climate models. We show how multifractal scaling laws can be extrapolated to small scales to learn about the nature of the mechanisms that accommodate the deformation. We stress that these scaling properties preclude the use of homogenisation techniques (i.e. the use of mean values) to link different scales, and we discuss how these detailed observations should be used to constrain sea ice dynamics modelling.***To cite this article: J. Weiss, D. Marsan, C. R. Physique 5 (2004).***

Résumé

Propriétés d'échelle de la déformation et de la fracturation de la banquise. La banquise, en isolant l'océan de l'atmosphère, joue un rôle fondamental dans le climat terrestre. Elle se déforme et se fracture sous l'action des vents, des courants océaniques et des contraintes thermiques. En sus des processus thermodynamiques, cette fracturation contrôle en grande partie la proportion d'eau libre et la distribution des épaisseurs de glace, deux paramètres très importants du point de vue climatique, particulièrement pendant l'automne et l'hiver en l'absence de fonte. Nous présentons ici une analyse des propriétés d'échelle de la banquise qui permet de caractériser l'hétérogénéité des réseaux de fracture et des champs de déformation, ainsi que l'intermittence des fluctuations de contrainte. Nous discutons les conséquences de ces propriétés d'échelle, en particulier pour la modélisation de la banquise dans les modèles climatiques. Nous montrons comment les lois d'échelle multifractales peuvent être extrapolées vers les petites échelles pour déterminer la nature des mécanismes physiques accommodant la déformation de la banquise. Nous soulignons le fait que ces lois d'échelle invalident l'utilisation de techniques d'homogénéisation pour modéliser les changements d'échelle, et nous discutons comment ces observations peuvent être utilisées pour contraindre des modèles de dynamique de la banquise. ***Pour citer cet article : J. Weiss, D. Marsan, C. R. Physique 5 (2004).***

* Corresponding author.
E-mail address: weiss@lgge.obs.ujf-grenoble.fr (J. Weiss).

1631-0705/$ – see front matter
doi:10.1016/j.crhy.2004.09.005

Keywords: Sea ice cover; Deformation; Fracture; Intermittency; Multifractal; Climate

Mots-clés : Banquise ; Déformation ; Fracture ; Intermittence ; Multifractal ; Climat

1. Introduction

Sea ice is a fundamental and fascinating component of polar regions. During winter, the sea ice cover extends over 14×10^6 km^2 of the Arctic ocean and surrounding seas and up to 20×10^6 km^2 around Antarctica. The variability of the sea ice extent between winter and summer is much larger in the southern hemisphere (less than 4×10^6 km^2 of sea ice during the austral summer) than in the Arctic where multiyear ice is important (7×10^6 km^2). When considered as a geophysical object, the Arctic sea ice cover is of the scale of tectonic plates.

Through complex interactions with the oceans and the atmosphere, sea ice, and particularly its extension and thickness, is a key parameter in the Earth's climate system. Sea ice insulates the ocean from the atmosphere. The fracturing and divergent deformation of the ice cover decrease the albedo and allow more shortwave absorption by the ocean, thereby shrinking the ice cover during summer, thus reducing its strength and possibly increasing the fracturing – a positive feedback loop (Moritz et al. [1]; Zhang et al. [2]). On the other hand, sea ice fracturing during winter enhances the production of new ice, and thereby modifies the heat and salinity budgets in polar regions (Maykut [3]). Within a context of global warming, these complex interactions between the ocean, sea ice and the atmosphere could be critical (Morison et al. [4]). Observations reveal that the Arctic sea ice cover already shrank during the last decades, both in terms of average thickness (Kerr [5]; Rothrock et al. [6]) or of geographical extension (Comiso [7]; Morison et al. [4]). These trends are expected to increase during the 21st century with strong climatic, environmental or economical consequences (Kerr [8]). Therefore, better characterization of sea ice deformation and fracturing, which is needed for better modelling, appears as an important scientific challenge for the next decades: how the ice cover evolves through time in response to meteorological and mechanical forcing, and how this in turn affects the Earth's climate, are still open questions. Climate models try to model these complex interactions (see, e.g., Fichelet and Morales Maqueda [9]). The sea ice modules of climate models necessarily simplify the ice dynamics, and particularly its spatial variability (see later). They are inspired from more specific, but more detailed sea ice dynamic models (see, e.g., Hibler [10]).

Beyond the climatic concerns, the sea ice cover is also a model geophysical object for studying deformation and fracture:

(i) The large aspect ratio of lateral extent to thickness ($\sim 10^6$ for the Arctic basin) allows the monitoring of the deformation of the ice cover from surface measurements; one can assume this process to be well approximated as a 2D plane stress mechanical problem at scales larger than few tens of m, i.e. at scales significantly larger than the ice cover thickness.
(ii) The physical and mechanical properties of saline ice are well documented at the laboratory scale (Cole [11]; Schulson [12]) and can be considered relatively homogeneous, at least compared to the structural heterogeneity of the Earth's upper crust.
(iii) Compared to the Earth's crust, sea ice motion and deformation occur at much shorter time scales, with 'typical' strain rates around 10^{-6} s^{-1} (although the concept of a 'typical' strain rate for a strongly heterogeneous velocity field is a matter of caution; see later). This enhances the signal/noise ratio and allows the sampling of the significant deformation mechanisms in a shorter time.
(iv) The absence of ground cover and the ability of imaging radar to penetrate clouds and darkness greatly facilitates the observation of deformation and fracturing.

For these various reasons, the available documentation on deformation and fracturing of the sea ice cover, especially in the Arctic, has no counterpart in geophysics. As an example, the available data on Earth's crust deformation obtained by interferometry or GPS are still much too sparse to allow the detailed scaling analyses of how shear zones accommodate the tectonic driving. We note that most of these data refer to the Arctic basin, the documentation about the sea ice cover around Antarctica being scarce (Geiger et al. [13]). Moreover, as the antarctic sea ice is mostly seasonal and unconstrained by land towards the north, its deformation features differ from arctic sea ice. Consequently, the present article focuses mainly on the Arctic.

As shown in this paper, deformation and fracturing processes of the sea ice cover are characterized by a strong spatial heterogeneity as well as intermittency:

(i) in space, most of the deformation is accommodated by leads, delimiting quasi-rigid floes (see for example Fig. 1(a));
(ii) in time, very large fluctuations in stress are observed, that correspond to strongly episodic sequences of fracturing and deformation (see for example Fig. 2).

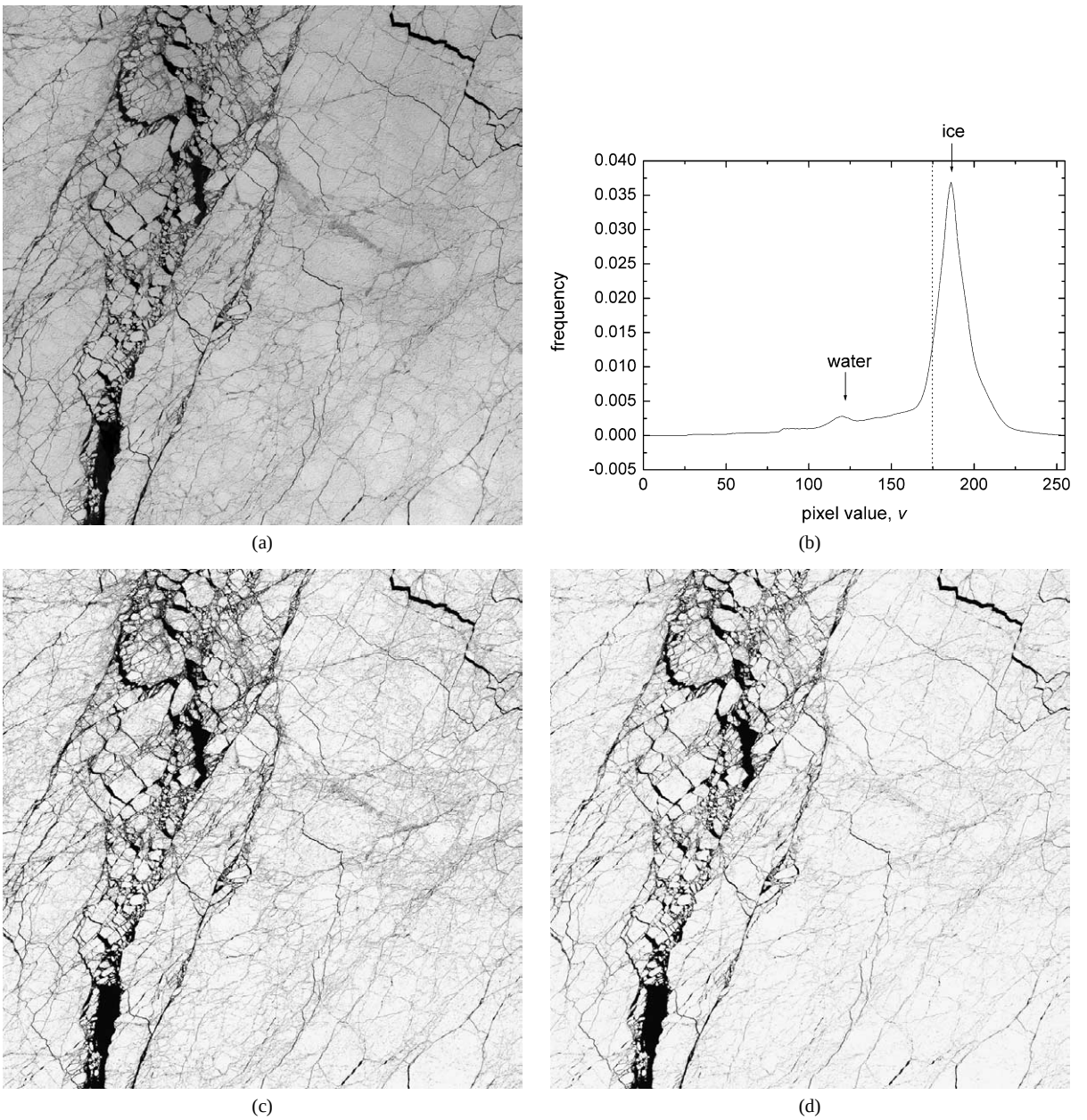

Fig. 1. (a) SPOT satellite grey-scale image of the sea ice cover taken the 6 April 1996, centred around N80°11′, W108°33′ and covering 59×59 km^2 with a resolution of 14.4 m/pixel. (b) Grey-scale histogram of the image plotted on (a). The dotted line represents the average value $\langle v \rangle = 176$. (c) Binary version of (a), using a threshold $v_{\text{th}} = 160$. (d) Binary version of (a), using a threshold $v_{\text{th}} = 140$.

Mean values of deformation, either in space or time, contain therefore very little information on the actual process that controls the evolution of the ice cover. In this respect, sea ice is similar to the Earth's crust that is also characterized by a strongly localized (faults) and intermittent (earthquakes) deformation. As explained below, this heterogeneity is observed over a very large scale range from the scale of the ice cover's thickness (m) to the scale of the Arctic basin (10^6 m), whereas intermittency is observed at least within the time scale 1 hour–1 year (Lewis and Richter-Menge [14]). Within those scale intervals, the deformation is observed not to favor any privileged scale that would mark a transition between different physical mechanisms acting in a scale-dependent way. (Note, however, that an opposite view can be found in McNutt and Overland [15]; Overland et al. [16].) Consequently, an essential, and still mainly open question in sea ice mechanics and modelling is to establish the

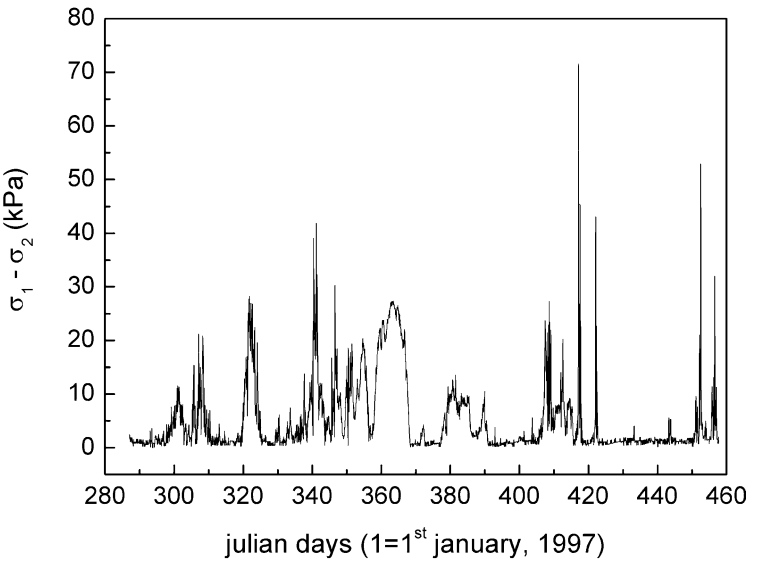

Fig. 2. Ice 'shear stress' $\sigma_1 - \sigma_2$ recorded from 14 October 1997 to 2 April 1998 at the Delaware bottom sensor during the SHEBA program. σ_1 and σ_2 are the 1st and 2nd principal stresses, respectively.

links between different scales (Schulson [12]; Schulson and Hibler [17]). This motivates our research on the scaling properties of deformation and fracture of sea ice.

This paper is organized as follows. Section 2 describes briefly the driving forces responsible for deformation and fracture of the ice cover as well as the boundary conditions. Section 3 presents a rapid overview of the scaling analyses presented in the sea ice literature and focuses on some new and particularly enlightening analyses. Section 4 discusses the consequences of these scaling properties, particularly for sea ice modelling in climate models. We show how multifractal scaling laws can be extrapolated to small scales to learn about the nature of the mechanisms that accommodate the deformation, or to correctly estimate the amount of open water within the ice cover. We stress that these scaling properties preclude the use of homogenisation techniques (i.e. the use of mean values) to link different scales, and we discuss how these detailed observations should be used to constrain sea ice dynamics modelling.

2. Driving forces

Strains, stresses and fracturing are induced in the sea ice cover by several driving forces, different in nature as well as in intensity (Lewis and Richter-Menge [14]):

(i) Wind forcing is responsible for motion-induced stresses and strains. This is generally considered to be the main forcing term of sea ice deformation. This forcing is known to be turbulent, the atmospheric flow being characterized by very large Reynolds numbers ($> 10^6$). As such, it is itself strongly varying in space and time, and is also scale invariant.
(ii) Ocean currents. This contribution is considered to be smaller than wind forcing. However, ocean drag on the bottom of the ice plays an important role in balancing the wind-induced velocities [14]. In the so-called marginal ice zone (MIZ) delimitating the ice cover from the open ocean, the ocean waves are known to play a role on the fragmentation of the cover. This mechanism becomes negligible several km from the MIZ. Near the coast, tides could also play a role.
(iii) Coriolis force. This term is considered to be small compared to the other terms [14].
(iv) A term related to the sea surface tilt induced by atmospheric pressure gradients. This term is very small compared to the other terms (Steele et al. [18]).
(v) Thermal strains and stresses induced by rapid variations of the air temperature (Lewis [19]) can result in tensile cracking of the sea ice cover. This mechanism is important for sea ice fracturing.

These different driving terms can be summarized in the following momentum balance equation (in a 2D modelling framework) which is at the root of most of the sea-ice dynamics models (see, e.g., Hibler [10,20]; Lindsay and Stern [21]):

$$m\frac{\partial u}{\partial t} = \tau_w + \tau_g - mf_c k \times u + \nabla \cdot \sigma \tag{1}$$

where m is the ice mass per unit area (2D modelling) and u the ice velocity. In this 2D framework, the sea surface tilt is neglected. τ_w and τ_g represent respectively the ocean and the wind 'stresses', i.e. forces per unit area. The third term represents the Coriolis force where f_c is the Coriolis parameter and k a unit vector normal to the surface. The last term is written in terms of the divergence of the internal ice stress tensor σ, which is a force per unit length in this 2D framework. σ is defined from a constitutive rheological law relating the displacement to the stress. Following Hibler [10], most of the sea ice dynamics models assume a viscous-plastic rheological law:

$$\sigma = 2\eta_b \frac{\mathrm{d}\varepsilon}{\mathrm{d}t} + \left[(\eta_s - \eta_b)T\left(\frac{\mathrm{d}\varepsilon}{\mathrm{d}t}\right) - \frac{P}{2}\right]I \tag{2}$$

where η_s and η_b are respectively the shear and bulk viscosities, $\mathrm{d}\varepsilon/\mathrm{d}t$ is the strain-rate tensor, $T(\cdot)$ the trace of a tensor, P the ice strength, and I the two-dimensional unity tensor.

For most of the Arctic ocean, the contribution of thermal stresses is small compared to wind forcing. Tensile fractures can open locally as the result of these thermal stresses, but the most significant fracturing features are associated with shear deformation. These 'faults' are called 'leads' in the ice literature. These mechanisms result in stresses that vary strongly in space and time. Lewis and Richter-Menge [14] reported values of up to 250 kPa, i.e. about the tensile strength of saline ice measured in the laboratory (200–300 kPa at $-3\,^{\circ}\mathrm{C}$ (Richter-Menge and Jones [22])). In case of areas shielded from strong winds and/or confined by coasts, such as fjords or bays, the relative contribution of thermal stresses and of ocean currents and tides can be larger.

3. Scaling of deformation and fracture of sea ice: observations

In a very broad sense, *scaling* designates the way an observable M changes with the scale of observation x. The scale x can be a spatial scale, a time scale, an energy scale. However, we employ here a more restrictive meaning originating from statistical physics (see, e.g., Stanley [23]): an observable (or distribution) M exhibits *scaling*, *scaling properties*, or *scale invariance* (all these terms are used in the literature) with respect to the scale x if $M(\lambda x)/M(x)$ only depends on the scale ratio λ but not on the resolution scale x, in the distribution sense. The notation λx can be understood in a broad sense (e.g., Lovejoy and Schertzer [24]) of a scale changing operator that only depends on the parameter λ. In the very simplest case, this yields $M(\lambda x) = \lambda^{\alpha} M(x)$ where α is the exponent associated with the function $M(x)$. The only function that satisfies the above equation is a power law, $M(x) \sim x^{\alpha}$ (in what follows, the sign '$\sim$' is used to indicate proportionality).

For now almost 20 years (Allègre et al. [25]; Barton and Larsen [26]), it has been progressively realized that deformation, fracture and faulting of the lithosphere is characterized by many different scaling properties including the self-affine geometry and multifractal properties of fracture surfaces (Power et al. [27]), power law distributions of fracture lengths, fractal distributions of fracture barycentres or earthquake hypo/epicentres, or scaling relations between fault lengths and fault slips (see, e.g., Main [28] or Bonnet et al. [29] for reviews on the subject). Power law distributions of earthquake energies (i.e. the Gutenberg–Richter law (Gutenberg and Richter [30]) and fractal correlation of earthquake occurrence times (Kagan and Jackson [31]) are another well-known scaling properties of the fracturing of the crust.

As detailed below, sea ice deformation and fracturing is characterized by multifractal scaling properties that describe the heterogeneity and intermittency of the processes over spatial scales ranging from the ice cover thickness (m) to the scale of the Arctic Basin (10^6 m), and time scales within the range 1 hour–1 year. We divided the available observations in three categories. Section 3.1 refers to 'static' observations (snapshots) in the sense that they describe the geometry of the ice cover (e.g., geometry of the fracture network) at a given time t. Section 3.2 presents observations based on 'kinematical' measurements such as displacements, velocities or deformations (e.g., displacement records of buoys, or Radarsat Geophysical Processor System (RGPS) data). Whereas static observations are common for the lithosphere, kinematic measures of the sea ice cover have yet no counterpart for other geophysical objects. Section 3.3 focuses on the intermittency of ice stress time series.

3.1. Static observations

As becomes obvious when seen from a plane or from space, the sea ice cover is not a uniform continuous sheet like the ice that might cover a small lake or a frozen pond. It is instead intensely fractured (Fig. 1(a)). On optical images, the large difference of albedo between thick ice and open water or thin ice allows one to easily identify recently opened fractures. During most of the year, fracturing is particularly concentrated along sets of leads, some of them extending over hundreds of km. Within these regions of intense fracturing, ice is fragmented into pieces called 'floes' (Fig. 1(a)). During summer, fragmentation of the ice cover into floes is more widespread and lateral melting plays a significant role, leading to an apparently more homogeneous pattern.

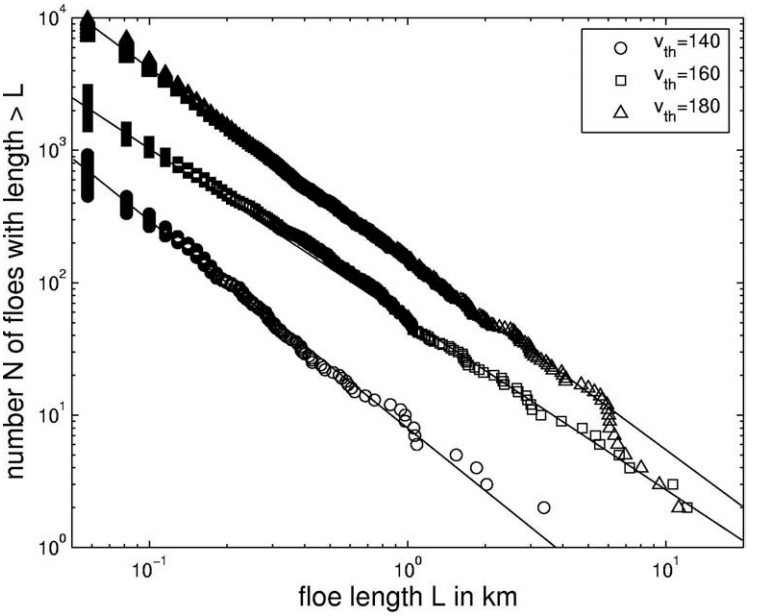

Fig. 3. Cumulative distributions of floes sizes, $N\ (>L)$, obtained after thresholding of the Fig. 1(a) with different thresholds $v_{\mathrm{th}} = 140$ (circles), $v_{\mathrm{th}} = 160$ (squares) and $v_{\mathrm{th}} = 180$ (triangles).

Historically, the first quantitative evidence of scale invariance of the fracturing of sea ice came from the analysis of the probability that a given floe has a characteristic length larger than length L, i.e. the cumulative distribution $f(L' > L)$, where the size L can be defined from a mean diameter or the square root of an area. Different authors reported power law distributions, $f(L' > L) \sim L^{-b}$, with b in the range 1.4–2.2 for L within the range 10^{-1}–10^{5} m (Kergomard [32]; Korsnes et al. [33]; Lensu [34]; Matsushita [35]; Rothrock and Thorndike [36]). This expresses scale invariance, as it is impossible to determine the scale of the image by comparing the relative number of floes of different sizes. Within the scale ranges analysed, none of these studies revealed crossover scales. A zone of intense fracturing during fall, winter or spring cannot be distinguished from summer pack ice on the basis of these scaling properties. As an example, Fig. 3 shows this scaling in the case of the SPOT image of Fig. 1(a), using various thresholds v_{th} for defining the floes: a floe is here a connected area of pixels with values v greater than v_{th}; see next section for a more detailed description of v. The cumulative distribution decays as L^{-b}, with b in the range 1.3 to 1.54 depending on the threshold v_{th}. A more detailed review on this subject is given in Weiss [38].

3.1.1. Multifractal characterization of sea ice fracturing

In what follows, we present an analysis of the heterogeneity of sea ice fracturing based on its scale invariant properties. We explore the scaling properties of a measure, the proportion (or 'density') of open water within the ice cover, p. This measure is a key parameter for climatic studies. It is introduced in sea ice modules of climate models as a concentration variable that depends on thermodynamics (heat budget), and on the ice cover dynamics through a conservation law that relates the rate $\mathrm{d}p/\mathrm{d}t$ to a divergence term $\nabla \cdot u$ (see, e.g., Fichelet and Morales Maqueda [9]). However, these models do not really simulate the mechanical effect of fracturing on the open water fraction p. As an example, an effect of the formation of leads by shear faulting is not taken into account. More specific sea ice dynamics models take into account more precisely these feedbacks of the deformation onto the open water fraction from parametrizations relating the evolution of p to divergence and shear (Stern et al. [37]).

The proportion, p, can be seen also as a fracture density and this analysis can be compared with similar analyses performed for the lithosphere (Ouillon et al. [39]), or for ice samples fractured in the laboratory (Weiss and Gay [40]). The analysis presented here is based on a grey-scale (0 for black to 255 for white) satellite SPOT image (visible wavelengths) of size 4096×4096 pixels with a resolution of $L_0 = 14.4$ m/pixel, centered around N80°11′ W108°33′, NW of Queen Elizabeth Islands, and taken 6 April 1996, i.e. in early spring conditions (Fig. 1(a)). The grey-scale value v of a pixel depends on the shade, i.e. on the roughness of the surface and the inclination of the solar light, and on the albedo of the surface. As the upper surface roughness of the ice cover, defined, e.g., as the standard deviation of the elevation, is very small (below the meter scale) compared to the horizontal scales explored (14.4 m to 59 km), v can be considered as a proxy of the albedo. However, as the incidence angle of the solar light is large at this latitude, an increase of v is observed, in average, from N to S over this very flat

surface, as the result of the Earth's surface curvature. Nevertheless, as ice has a very high albedo compared to water, the image histogram is characterized by two well-defined peaks (Fig. 1(b)) at about $v = 120$ (water) and $v = 185$ (ice). This allows one to deduce p from v on a binary version of the image, using a threshold v_{th} in the 120–185 interval delimited by the two peaks of Fig. 1(b). Pixels with $v \leqslant v_{\text{th}}$ are approximated to be water or thin, transparent ice ($p = 1$), pixels with $v > v_{\text{th}}$ are ice ($p = 0$). Note, however, that some small and narrow dark lineaments could correspond to pressure ridges (compressive fracture). In this case, $p = 1$ would be associated to fractures but not to open water. The binary version of the grey-scale image of Fig. 1(a) for $v_{\text{th}} = 160$ and $v_{\text{th}} = 140$ are shown respectively on Figs. 1(c) and (d).

A first indication of the scale invariance of the grey-scale image (Fig. 1(a)) is given in Fig. 3, for which individual floes were singled out after thresholding, for $v_{\text{th}} = 140$, 160 and 180. In order to further test the scale invariant character of this image before introducing the threshold parameter (v_{th}), we compute the 2D spatial spectrum $v(\kappa_x, \kappa_y)$ and sum it along shells of radius κ (Fig. 4). This implicitly assumes the isotropy of the distribution, i.e. that both x and y directions are individually characterized by the same 1D spectrum. This was checked beforehand to be well verified. A very clear $1/\kappa$ scaling is observed, in the scale interval extending from 100 m to 10 km.

This result demonstrates the scale invariance of the image, but is difficult to interpret directly in terms of sea ice fracturing, as the pixel value v expresses composite information (see above and Section 3.1.2). Consequently, we focus now on binary images. We define a binary ice/water image $p(x, y)$ at the 14.4 m resolution scale, and examine its scaling properties by spatially averaging it at scale L:

$$\begin{aligned} &p(x, y) = 0 \quad \text{if } v(x, y) > v_{\text{th}}, \\ &p(x, y) = 1 \quad \text{if } v(x, y) \leqslant v_{\text{th}}, \text{ at the resolution scale } L_0, \\ &p_L(x, y) = \iint \mathrm{d}x' \, \mathrm{d}y' \, p(x - x') p(y - y') B_L(x', y') \end{aligned} \tag{3}$$

where B_L is a spatial averaging kernel with characteristic scale L. We here take B_L to be zero everywhere except within a square of size L centered at the origin. The quantity p_L can be considered as the fraction of open water when observed at scale L, and with an image resolution $L_0 \leqslant L$. Its distribution changes with the averaging scale L. The distribution can be studied by estimating the scaling of the moments $\langle p_L^q \rangle$, where $\langle \cdot \rangle$ stands for average. This is done for $0 \leqslant q \leqslant 3$. For the image thresholded at $v_{\text{th}} = 160$ (Fig. 1(c)), a $\langle p_L^q \rangle \sim L^{-K(q)}$ scaling is observed over about 2.5 orders of magnitude (0.2 km $\leqslant L \leqslant$ 60 km), see Fig. 5(a). However, a spurious effect arises towards small scales on the binary image: $\langle p_{L_0}^q \rangle = \langle p \rangle = 0.148$ whatever q for $L_0 = 14.4$ m $= 1$ pixel, as p_L takes only the values 0 or 1 at this scale. An effect of the image resolution is also possible. These effects significantly bends the scaling over about one order of magnitude (Fig. 5(b)). Similar departures from scaling were observed on simulated multiplicative cascade models, after thresholding of the distribution at resolution scale.

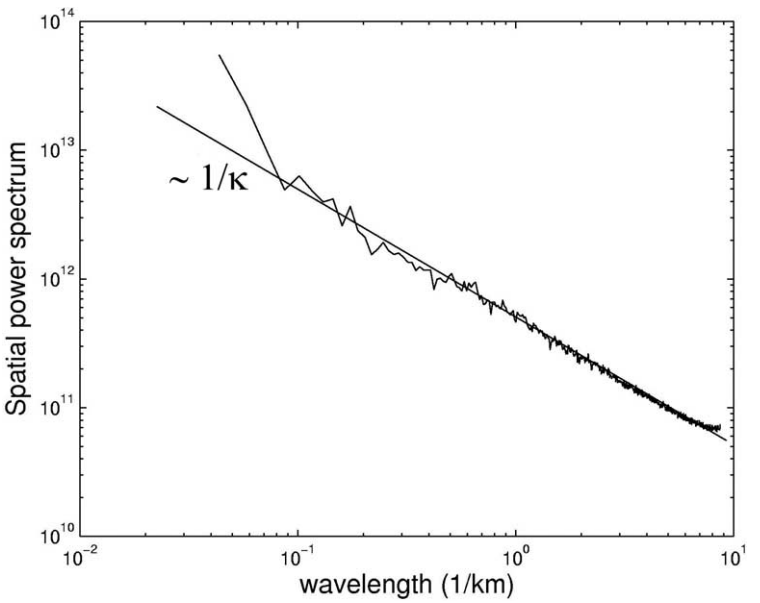

Fig. 4. 2D spatial spectrum of the grey-scale image of Fig. 1(a), summed along shells of radius κ. The $1/\kappa$ scaling is shown as a straight line.

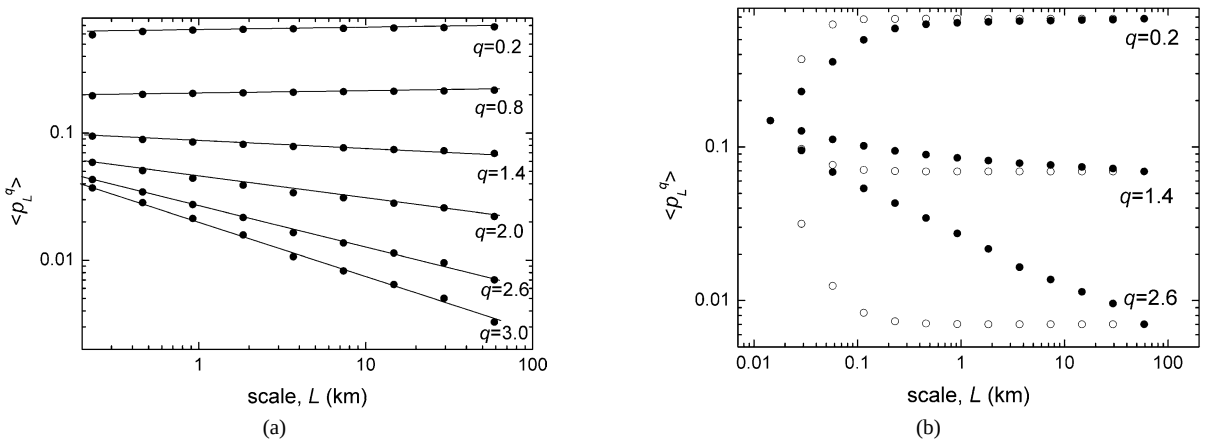

Fig. 5. Multifractal analysis of the density of open water, p_L, for the image thresholded at $v_{\text{th}} = 160$ (Fig. 1(c)): (a) moments $\langle p_L^q \rangle$ as a function of scale L for different values of q over the scale range 0.2–60 km, and the least squares lines. The slopes of these lines are $-K(q)$: (b) moments $\langle p_L^q \rangle$ as a function of scale L for $q = 0.2$, $q = 1.4$ and $q = 2.6$ over the whole available scale range 0.0144–59 km (closed symbols), along with the same moments for a randomly reshuffled image (open symbols). See text for details.

To test the significance of the observed scaling, we compare the results with a similar analysis performed on a randomly reshuffled image containing the same number of 'fractured' (black) pixels (Fig. 5(b)). In this case, the same constraints apply to $\langle p_L^q \rangle$ at $L_0 = 1$ pixel, i.e. $\langle p_{L_0}^q \rangle = \langle p \rangle = 0.148$. At the other bound ($L = L_{\max} = 59$ km), there is only one cell, so $\langle p_L^q \rangle = p_{L_{\max}}^q$ depends only on q and is identical for the initial image and the reshuffled data. Nevertheless, between these two commons bounds, the actual behavior of $\langle p_L^q \rangle$ is clearly seen to depart from the random test. This allows us to conclude that the observed scaling $\langle p_L^q \rangle \sim L^{-K(q)}$ is not inherent to the binary version of the image, but is a signature of the spatial correlations present in the fracture network.

The closed symbols in Fig. 6 shows the evolution of $K(q)$ vs q for the image thresholded at $v_{\text{th}} = 160$. A strong curvature is observed, indicating multifractality of sea ice fracturing. In comparison, a monofractal field would lead to a linear $K(q)$. With the present definition of the fracture density p, the function $K(q)$ is constrained by $K(1) = 0$, as $\langle p \rangle = 0.148$ whatever the scale, and $K(0) = 0$. The convexity of $K(q)$ implies that the higher moments of the distribution, which correspond to the largest values of p_L, grow faster towards small scales than for a monofractal scaling, as $K(q_2) > K(q_1) \times q_2/q_1$ for $q_2 > q_1$ (Marsan and

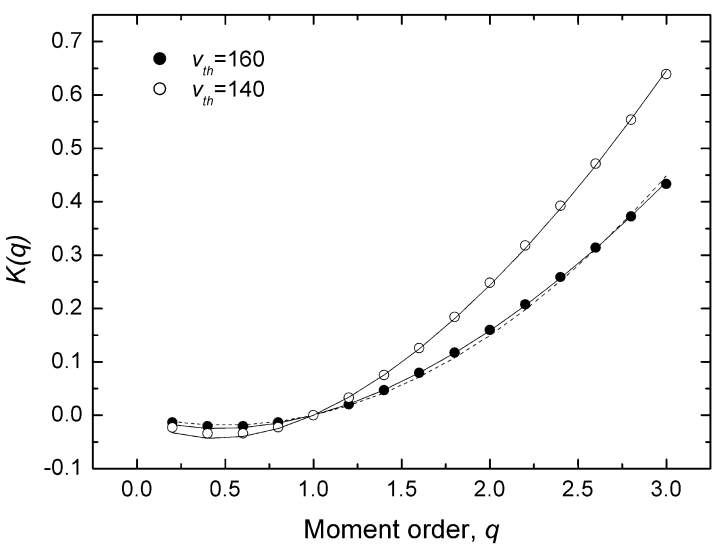

Fig. 6. Experimental moment function $K(q)$ for p_L. Closed circles: for the image thresholded at $v_{\text{th}} = 160$ (Fig. 1(c)). Full line: best-fit of the data with the Universal Multifractal Model ($\alpha = 1.67$). Dashed line: fit of the data with the lognormal model ($\alpha = 2$). Open circles: for the image thresholded at $v_{\text{th}} = 140$ (Fig. 1(d)). Full line: best-fit of the data with the Universal Multifractal Model ($\alpha = 1.50$).

Bean [41]). Therefore, the heterogeneity of sea ice fracturing increases towards small scales, i.e. fracturing is more localized. As an example, the standard deviation of p_L is given by $\sigma_{p_L} = (\langle p_L^2 \rangle - \langle p_L \rangle^2)^{1/2}$, hence scales as $(L^{-K(2)} - 0.148^2)^{1/2}$ and therefore increases towards small scales. However, the analysis shows that the mean and the standard deviation of p_L are not sufficient to determine the spatial distribution of sea ice fracturing, which is non-Gaussian.

Even though a similar multifractal behavior is obtained when changing the threshold v_{th}, the exponents $K(q)$, i.e. the pdf of p_L, are seen to be threshold-dependent. Fig. 6 shows a comparison between the $K(q)$'s obtained for $v_{\text{th}} = 140$ and $v_{\text{th}} = 160$. This shows the difficulty of unambiguously determining the fraction of open water from observations under visible light, as the pdf of p_L not only depends on the observation scale L, but also on the chosen threshold v_{th}.

3.1.2. Multifractal modelling with random multiplicative cascades

An analytical expression of the moment function $K(q)$ can be proposed within the multifractal modelling framework based on the concept of random multiplicative cascades, which was initially developed in turbulence to account for and model scale invariance and correlations of the energy flux (see, e.g., Frisch [42]). The generation of multifractal distributions from multiplicative cascades has been detailed elsewhere (see, e.g., Marsan and Bean [41]; Schertzer et al. [43] for reviews). We summarize here the basic concepts for a 2D situation (particularly suited for sea ice modelling; see Section 1). The construction of a multiplicative cascade is a down-scaling procedure starting from an upper scale $L_{\max}$ (the scale of the 'system') down to a lower scale $L_{\min}$. This lower scale can be a resolution scale (we are unable, with our observation tools, to resolve fluctuations and heterogeneity at scales $L < L_{\min}$), or can be related to a physical cut-off when the physical parameter under consideration (e.g., the fraction of open water p) is only slowly varying at scales below $L_{\min}$. In turbulence, this lower cut-off is the so-called dissipation scale, at which viscosity terms in the Navier–Stokes equation start to become dominant over advection. Multiplicative cascades fragment the value of the parameter M from $L_{\max}$ to $L_{\min}$ in a scale invariant way illustrated on Fig. 7. The value M_L at scale L is divided into 4 smaller values $M_{L/2}(1), \ldots, M_{L/2}(4)$ at scale $L/2$ with intensities given by $M_{L/2}(i) = M_L f_i$, where f_i are independent realizations of a positive random variable f. It is easy to see that multiplicative cascades generate scale invariant and correlated fields (the value $M_L(i)$ at scale L and location i is correlated to the value at location j through N generations of 'parents', where N depends on the logarithm of the distance $|i - j|$ and on the scale ratio $L_{\max}/L$).

Within this general framework, there is no a priori constraint on the nature of the positive random variable f. However, the so-called 'universal' multifractal model introduced by Schertzer and Lovejoy [44] has found a wide applicability for describing the scale properties of many geophysical fields, as for example atmospheric turbulence (Schmitt et al. [45]), rainfall (Schertzer and Lovejoy [44]), climatic records (Schmitt et al. [46]) or upper crustal properties (Marsan and Bean [41]). This model is based on log-Lévy statistics for f, and is therefore a limit process since the sum of independent, identically distributed random variables converge towards Lévy laws. The moment function $K(q)$ takes the analytical form:

$$K(q) = \frac{C}{\alpha - 1}\left(q^{\alpha} - q\right) \tag{4}$$

where C and α are constants ($0 \leqslant \alpha \leqslant 2$). The Lévy index α characterizes the degree of multifractality. $\alpha = 0$ corresponds to a monofractal whereas $\alpha = 2$ is associated with the lognormal model where f is a lognormal random variable.

The fits obtained with Eq. (4) for the experimental moment functions $K(q)$ describing the fracture patterns of Fig. 1(c) ($v_{\text{th}} = 160$) and (d) ($v_{\text{th}} = 140$) are shown in Fig. 6. The best fit is obtained with $C = 0.090$ (respectively 0.147) and $\alpha = 1.67$ (1.50) for $v_{\text{th}} = 160$ (respectively $v_{\text{th}} = 140$). This shows that sea ice fracturing can be modelled by a multiplicative cascade process with a degree of multifractality slightly lower than the lognormal model. However, this deviation from the lognormal model is small, as shown on Fig. 6. The parameters of the multiplicative cascade change with the threshold v_{th}, with a decreasing degree of multifractality α with decreasing threshold.

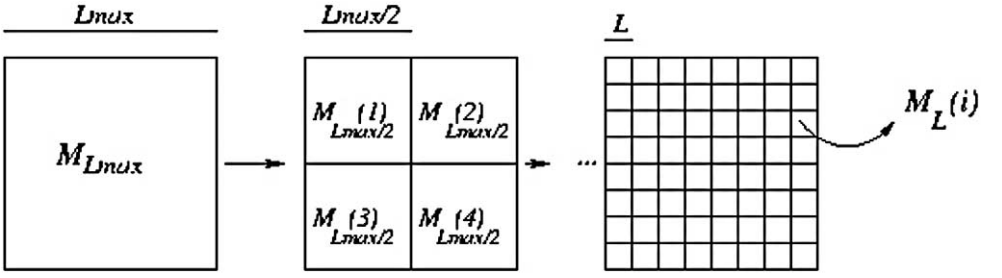

Fig. 7. Construction of a multiplicative cascade model (see text for details).

It is worth mentioning here that the multifractal analysis performed on the image as well as the cascade model proposed are isotropic and as such cannot reveal (or model) any directional information, even though clear anisotropy is seen (quasi-linear leads) on the image (Figs. 1(a), (c) and (d)).

Instead of using a threshold to binarize the image, one could perform a multifractal analysis directly on the pixel value v, i.e. on a proxy of the albedo. However, the physical interpretation would be difficult for several reasons. Thin ice freshly formed along fractures has an albedo intermediate between water and thick (~ 1 m) ice, but the relation thickness-albedo is still an open, and probably very complex question. Indeed, in addition to ice thickness, albedo strongly depends on others physical parameters such as the amount of snow covering the ice. Moreover, we already stressed the role of the Earth's surface curvature on v. A multifractal analysis on v shows reasonable scaling of the moments $\langle v^q \rangle$ towards large scales, but significant deviations towards small scales that probably reflect this composite information. Falco et al. [47] performed a similar multifractal analysis of the backscatter amplitude of synthetic aperture radar (SAR) images of sea ice. SAR backscatter amplitude relates to other physical properties different from the albedo in the visible wavelength range, such as the thickness, the bulk properties (e.g., the brine content), the roughness of the surface, the salinity, etc. The SAR backscatter fields analysed were well described as a universal multifractal with $C = 0.0086$ and $\alpha = 1.85$ over the scale range 12.5 m–6.4 km. Owing to the composite information carried by the SAR backscatter, this result is difficult to interpret in terms of deformation and fracture.

The most detailed multifractal analysis of fracturing and faulting of the Earth's crust was presented by Ouillon et al. [39]. This was performed from box-counting on several fault and fracture trace maps in Saudi Arabia from the 1 cm to the 100 km scale. Compared to the analysis presented above, several complications arose: (i) the analysis is based on 2D information although the crust thickness clearly cannot be neglected; (ii) the fracture traces result from an interpretation of the observer and are modelled as lines; and (iii) sediment layers can hide the pattern in some places, leading to sampling bias. Instead of using a fracture density as defined above, Ouillon et al. [39] considered an extensive measure, i.e. the fracture length cumulated over the box, and characterized the multifractal properties by a set of generalized fractal dimensions $D(q)$. It is easy to show that $D(q) = 2 - (K(q)/q - 1)$. This analysis revealed multifractal scaling of crustal fracture patterns over limited scale ranges separated by crossover scales possibly associated with the layering of the crust. This interpretation is consistent with the absence of such characteristic scales for the sea ice cover within the scale range 10–10^4 m, well above the ice cover thickness (see Section 4.1).

3.2. Kinematic observations

As we stressed above, high-resolution and spatially dense kinematic measures such as velocities or deformations can be derived from buoys or satellite imagery of the sea ice cover. Expanding our view from purely static distributions, this allows us to analyse the scaling properties of the strain and strain-rate fields.

3.2.1. Dispersion of buoys

Martin and Thorndike [48] studied the deformation of sea ice from the dispersion of buoys. They measured the squared separation of buoys averaged over many pairs, $\langle \Delta L^2 \rangle$, as a function of time t. For classical (molecular) diffusion, $\langle \Delta L^2 \rangle \sim t$. For turbulent Lagrangian diffusion, two regimes are present with $\langle \Delta L^2 \rangle \sim t^2$ for small time scales and $\langle \Delta L^2 \rangle \sim t$ for large time scales (Taylor [49]). The observations reported by Martin and Thorndike [48] were in this respect in reasonable agreement with turbulent diffusion. Moreover, the dispersion rate $\mathrm{d}\langle \Delta L^2 \rangle / \mathrm{d}t$ increases with the separation L as $\mathrm{d}\langle \Delta L^2 \rangle / \mathrm{d}t \sim L^\delta$, with $\delta = 1.1$ for small time scales (few hours) and $\delta = 1.8$ for large time scales (few days). This strongly differs from classical diffusion (no scaling, i.e. $\delta = 0$), but resembles the turbulent scaling, although the latter is characterized by different exponents (2/3 and 4/3 for respectively small and large time scales (Richardson [50]). All of this suggests a kind of 'solid turbulence' where dispersion within the sea ice cover is essentially the result of fracturing. Recast in terms of deformation, these results show that the moment of order 2 of a strain-rate, $\mathrm{d}\langle (\Delta L/L)^2 \rangle / \mathrm{d}t^2$, scales as $L^{\delta-2}$, therefore increases with decreasing spatial scale. More precisely, Martin and Thorndike [48] analysed the scale dependence of the components of $\langle \Delta L^2 \rangle$ normal and parallel to the line initially joining the two points, and found the same exponents. However, as with turbulence, we show below that the first and second order moments of the dispersion rate are not sufficient to characterize the strain-rate field of sea ice.

3.2.2. Deformation from RGPS

The RADARSAT Geophysical Processor System (RGPS) has allowed in recent years the investigation of sea ice motion and deformation over an unprecedented range of scales, from 10 km to the scale of the Arctic Ocean as a whole (≈ 1000 km). RGPS is based on a cross-correlation technique applied to consecutive SAR images (Fily and Rothrock [51]), which allows tracking in a Lagrangian fashion more than 40 000 points over the Arctic during an entire season. The tracked points define the corners of cells which are initially square (10×10 km). The velocities of the cell corners (u, v) are computed over the period between two observations (typically 3 days) and are used to calculate the velocity gradients for each cell. This allows computation of the

strain-rate tensor for each cell, a database that has no counterpart in geophysics. Details about RGPS can be found elsewhere (Kwok [52]; Kwok et al. [53]).

Recently, Marsan et al. [54] performed a multifractal analysis of sea ice deformation from the RGPS database. For a 3-day interval centered around 5 November 1997, they computed the scaling of the moments $\langle(\mathrm{d}\varepsilon/\mathrm{d}t)^q\rangle$, where the so-called total strain rate $\mathrm{d}\varepsilon/\mathrm{d}t$ was defined as $\mathrm{d}\varepsilon/\mathrm{d}t = ((\partial u/\partial x - \partial v/\partial y)^2 + (\partial u/\partial y + \partial v/\partial x)^2)^{1/2}$. This scalar quantity contains information about the intensity of the strain-rate, whereas the information about the principal directions is lost. In this case, the mean $\langle\mathrm{d}\varepsilon/\mathrm{d}t\rangle$ is not necessarily constant with scale, as the strain-rate is not necessarily conservative. Indeed, Marsan et al. [54] observed a power law decrease of $\langle\mathrm{d}\varepsilon/\mathrm{d}t\rangle$ with increasing scale, $\langle\mathrm{d}\varepsilon/\mathrm{d}t\rangle \sim L^{-0.20}$. They reported a strong curvature of the experimental moment function $\beta(q)$, i.e. $\langle(\mathrm{d}\varepsilon/\mathrm{d}t)^q\rangle \sim L^{-\beta(q)}$, indicating multifractality of the strain-rate. $\beta(q)$ was very well approximated by a quadratic fit, $\beta(q) = aq^2 + bq$ with $a = 0.13$ and $b = 0.068$. This means that the strain-rate can be modelled by a lognormal multiplicative cascade. However, as the strain rate is not conservative ($\beta(1) \neq 0$), the multifractal model of Eq. (4) cannot be directly applied (further fractional integration of a conservative cascade would be necessary). As for the fracture density p, the strain-rate becomes more localized towards small scales. The similarity between the scaling behaviours of the strain-rate and of the fracture density is certainly not coincidental. It expresses the fact that deformation drives the fracture process whatever the scale. It suggests also that brittle deformation (fracture opening, faulting, ...) is essential in sea ice mechanics.

This scaling behaviour of the strain-rate is in qualitative agreement with the dispersion of buoys reported by Martin and Thorndike [48], although the value of $\beta(2) = 0.66$ obtained for $\mathrm{d}\varepsilon/\mathrm{d}t$ is larger than the exponent obtained for $\mathrm{d}\langle(\Delta L/L)^2\rangle/\mathrm{d}t^2$ at large time scales ($|\delta - 2| = 0.2$; see Section 3.2.1).

We stressed at the end of Section 3.1.1 the difficulty of unambiguously determining the open water fraction p from an optical, static image. Stern et al. [37] have used a thresholding of kinematical (e.g., divergent motions greater than a threshold) rather than static data to define newly formed open water regions. These data were used to parameterize the relation between p and strain in sea ice dynamics models. However, the thresholding of a multifractal strain field raises ambiguities similar to those reported in Section 3.1.1.

3.3. Dynamical observations: intermittency of the deformation process

So far, we have analysed the heterogeneity of sea ice fracture and deformation in the spatial domain. However, these processes are also strongly irregular in the time domain: as with the Earth's crust, the deformation is accommodated during short-duration events (fracturing episodes) that relate to the brittle character of sea ice (e.g., Dudko et al. [55]). Sea ice stresses monitored over several months by stress gauges frozen into the ice cover during the Sea Ice Mechanics Initiative (SIMI) field program (Lewis and Richter-Menge [14]; Richter-Menge and Elder [56]), also exhibited a strong intermittency. Similar measurements have been performed more recently during the Surface Heat Budget of the Arctic Ocean (SHEBA) program, north of the Alaskan coast (see http://sheba.apl.washington.edu). In what follows, we analyse the scaling properties of one of these records, kindly provided by J. Richter-Menge and B. Elder from CRREL (see also http://www.joss.ucar.edu/sheba). This 'shear stress' record τ (here defined as the 1st principal stress minus the 2nd) was recorded at a sampling rate of 1 hour starting from 14 October 1997. Our analysis is based on the first 4097 data points of the series (i.e. about 171 days) plotted on Fig. 2, which shows the intermittent character of the ice stresses. As shown on Fig. 8, the power spectrum $E(F)$ of the stress record is scale invariant in time, $E(F) \sim F^{-\mu}$, where F is the frequency and $\mu = 1.42$ in the present case. Note that no well-marked peak can be seen neither at tidal nor inertial time scales. The fact that the algebraic slope of the power spectrum is less than -1 indicates that the time series is a non-conservative fractal. Consequently, as for example with classical fractional Brownian motion (Mandelbrot and Van Ness [57]), we analyse how the distributions of the increments $\tau(t + \Delta t) - \tau(t)$ vary with the time scale Δt. We performed a multifractal analysis by calculating the moments of this shear stress increment (positive or negative) defined as:

$$\langle \Delta\tau^q \rangle = \langle |\tau(t + \Delta t) - \tau(t)|^q \rangle \tag{5}$$

where Δt is a time increment. We used the time scales $\Delta t = 2^n$ hours with n varying from 1 to 12. The results are plotted on Fig. 9. A scaling behavior $\langle \Delta\tau^q \rangle \sim \Delta t^{\zeta(q)}$ is observed over more than two orders of magnitude, from $\Delta t = 1$ hour to more than 10 days. The break observed around 300 hours is an artefact of the analysis due to a finite size effect and is not recovered in the power spectrum (at $F \approx 0.08$ day^{-1}; see Fig. 8). The moment function $\zeta(q)$ plotted on Fig. 10 shows curvature, i.e. multifractality in the time domain. Theoretical arguments lead to $\zeta(2) = \mu - 1$ (see, e.g., Frisch [42]; in the case of velocity increments in turbulence), in correct agreement with our results, $\zeta(2) = 0.47$ and $\mu = 1.42$.

The quantity $\langle \Delta\tau \rangle / \Delta t$ can be seen as a stress rate measured at the time scale Δt. It scales as $\Delta t^{-0.66}$, as $\zeta(1) = 0.34$, hence increases with decreasing time scale. The moment function of the stress rate, $\zeta(q) - q$, expresses the intermittency of the stress fluctuations. As the higher moments of the stress rate distribution growth faster towards small scales than for a monofractal scaling, the stress record is increasingly 'localized' in time towards small scales.

We noted in Section 3.2.1 that Martin and Thorndike [48] reported observations on the square separation of buoys, $\langle \Delta L^2 \rangle$, in reasonable agreement with turbulent diffusion, i.e. $\langle \Delta L^2 \rangle \sim t^2$ for small time scales (few hours) and $\langle \Delta L^2 \rangle \sim t$ for large

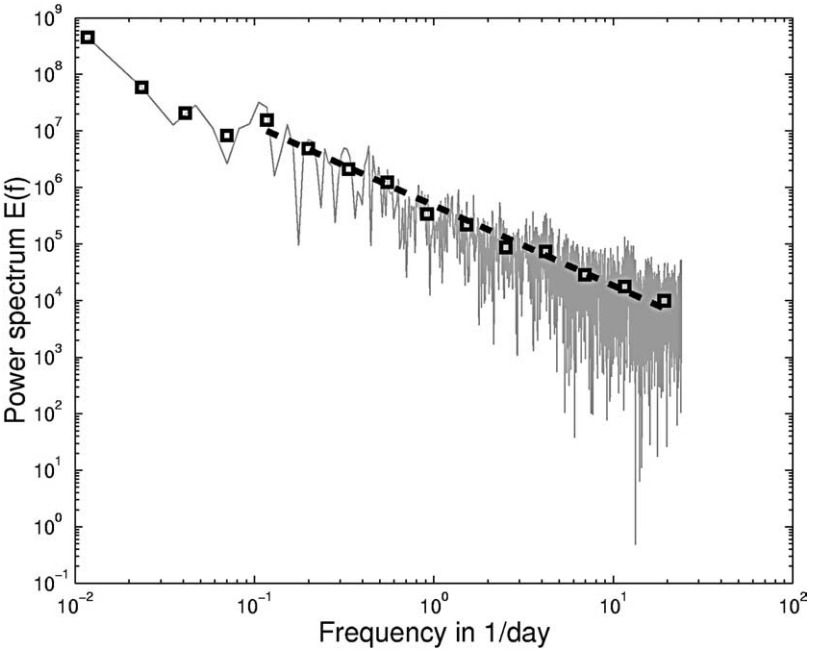

Fig. 8. Power spectrum of the shear stress record of Fig. 2 (in light grey). A power-law fit (thick dashed line) is estimated by averaging the spectrum over frequency windows with algebraically increasing width (squares), yielding $E(F) \sim F^{-\mu}$, with $\mu = 1.42$.

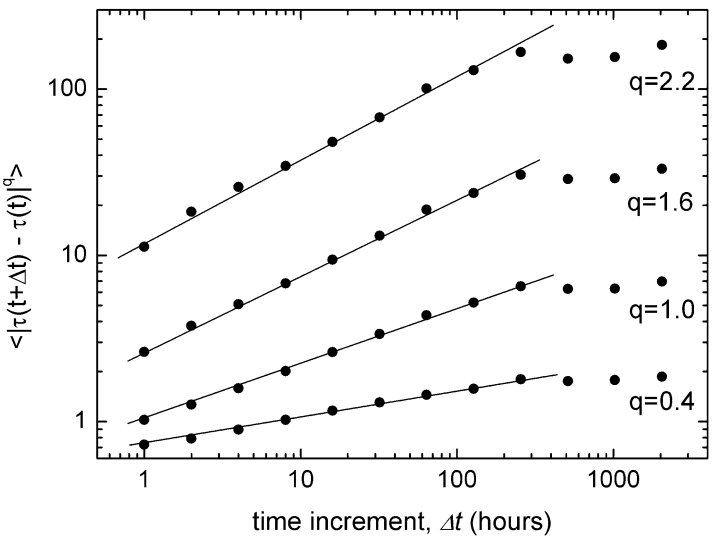

Fig. 9. Moments $\langle |\tau(t + \Delta t) - \tau(t)|^q \rangle$ as a function of the time scale Δt for different values of q over the range 1–4096 hours, and the least squares lines.

time scales (few days). Recast in terms of strain rate, this means that the moment of order 2 of the strain rate, $\langle (\Delta L/L)^2 \rangle / \Delta t^2$, is independent of Δt for small time scales, and scales as Δt^{-1} at large time scales. This Δt^{-1} scaling can be compared with a $\Delta t^{-1.53}$ scaling observed for the moment of order 2 of the stress rate ($\zeta(2) - 2 = -1.53$). The first regime $\langle \Delta L^2 \rangle \sim t^2$ giving a well-defined separation velocity is not observed here in the range 1 hour – 170 days. The transition between the two regimes is expected to occur at much shorter time scales than the few hours of Martin and Thorndike [48] as it should scale with the spatial scale at which it is measured (several km for Martin and Thorndike [48], several centimetres for the stress gauge which data are analysed here).

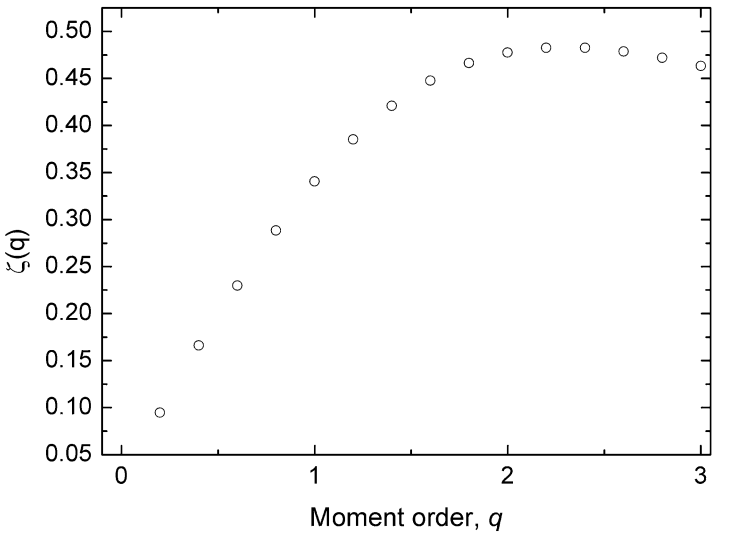

Fig. 10. Experimental moment function $\zeta(q)$ for $|\tau(t+\Delta t)-\tau(t)|$.

It would be interesting to document, in future similar experiments, how the peak stress fluctuations relate to episodes of fracturing, for example surveyed by seismological instrumentation.

4. Discussion

4.1. Origin of multifractality

We have shown that the observables, either static (e.g., fracture density) or kinematic (strain rate), associated with sea ice deformation are characterized by a multifractal scaling and can be modelled by multiplicative cascades. We stress again that we analysed scalar fields, ignoring the directional or tensorial information. Indeed, multifractal analysis of vectorial or tensorial fields (displacement and strain) need to be developed in the case of the sea-ice cover.

As explained in Section 2, the turbulent winds represent the main driving force for sea ice deformation. Both the forcing (winds) and the response to it (deformation of the ice cover) exhibit multiscaling properties. Marsan et al. [54] stressed this similarity, especially when the multifractality of the strain-rate is recast in terms of velocity (i.e. $\mathrm{d}\varepsilon/\mathrm{d}t \times L$) and compared to turbulent velocity fields (Frisch [42]). This could suggest that the turbulent, multifractal driving causes the deformation to be multiscaling as well.

On the other hand, multifractal fracture patterns have been observed for the Earth's crust (Ouillon et al. [39]), although plates motion which drives crustal deformation is not turbulent. Cowie et al. [58] developed a 2D numerical lattice model of fracturing. They applied spatially homogeneous antiplane shear deformation and observed the development of an heterogeneous fracture network with multifractal properties of the displacement field. Cowie et al. [58] argued that multifractality arose from the combination of three ingredients: long-ranged elastic interactions, a threshold mechanism for the rupture of the elements, and the presence of noise in the system (e.g., the rupture threshold of the elements). These three ingredients apply to sea ice fracturing, in addition to a multifractal driving (the winds). It is therefore difficult at this stage to discriminate the respective roles of these different parameters without the development of new numerical simulations.

As noted above, the main difference observed in terms of multifractality between sea ice and crustal deformation is the presence of crossover scales related to layering of the crust. Layering can be present within sea ice, especially in multiyear ice. However, this occurs at scales necessarily below the ice cover thickness and therefore does not leave any fingerprint on the scaling at much larger scales. In turbulence, scaling holds down to the dissipation scale where diffusion becomes important. For sea ice, the scaling is probably lower-bounded by the crystal scale (mm–cm) and the cover thickness (m), within a scale range where uncorrelated spatial fluctuations of the ice properties occur (crystal orientation and size, brines, layers, ...).

4.2. Consequences of the scaling properties

Even if the origin of the multifractality of sea ice deformation is still unclear, these scaling properties have important consequences in terms of sea ice modelling and for the interpretation of observations.

Scaling implies that small scales cannot be arbitrarily disconnected from larges ones. Consequently, homogenization, which assumes that an intensive measure, such as a density, can be considered as independent of scale above an elementary representative scale, is not relevant for sea ice mechanics. As an example, we have shown in Section 3.2 that the average strain-rate $\langle \mathrm{d}\varepsilon/\mathrm{d}t \rangle$ decreases towards large scales up to the scale of the entire Arctic Basin. Overland et al. [16] proposed a hierarchical theory of sea ice mechanics based on the distinction of disconnected scale intervals, delimited by characteristic scales related to typical crystal scale, floe scale, and so on. Hierarchy theory assumes that it is the degree of disconnection of processes between different scales that constitutes the organization of the system. It explicitly uses homogenization to make the links between these different scales. This is in contradiction with the multifractal scaling detailed above.

Let us consider now the modelling of sea ice within climate models. Their typical grid resolution is around tens of km for regional models (Gallée [59]) and can vary spatially for global climatic models between tens and hundreds of km (Fichelet and Morales Maqueda [9]). As noted above, the fraction of open water over the sea ice cover, p, is a key parameter of these models. For example, it is used to calculate the ice strength P. However, the possible feedbacks are ignored or simplified, as p is determined only from thermodynamic processes and from a divergence term (see Section 3.1.1). Moreover, the open water fraction p (and consequently all the related parameters, including the ice strength P) are considered in such models within a continuous framework, that is a value is assigned to each grid point. This implies that the sub-scale variability of p, i.e. at scales smaller than the grid resolution, is not important, in disagreement with the observations reported here.

As atmosphere-ice-ocean interactions are complex and often non-linear processes, this ignorance of a sub-grid scale variability of p can be misleading. As an example, following Hibler [10], the ice strength P is parameterized in most of the climate models as:

$$P = P^* h(1-p)e^{-Cp} \tag{6}$$

where h is the ice thickness and P^* and C are empirical constants. Because of the non-linearity of (6), to neglect the non-Gaussian statistics and the sub-scale variability of p can lead to a mis-estimation of P. This mis-estimation will increase with the degree of non-linearity of the process as well as with the ratio between the grid resolution (tens to hundreds km) and the lower bound of scaling (around the meter scale, see above). The same is true for other model variables such as thermodynamic fluxes that depend on both p and h. Although the determination of the ice thickness h, and its spatial variability from satellite imagery is still an open question, the scaling properties of both the pixel value v (Fig. 4) and p (Section 3.1) suggest non-Gaussian, possibly scale invariant statistics for h.

If the spatial variability of p, h or $\mathrm{d}\varepsilon/\mathrm{d}t$ is an issue, the intermittency revealed in Section 3.3 could be another one. The time step of climatic simulations is of the order a day and the forcing fields of the models such as the geostrophic winds are also averaged over a day. Time averaging of processes which are known to be intermittent at least down to the hour scale could therefore raise problems.

From the scaling analyses presented here, one could suggest possible directions for the improvement of sea ice modelling in climate models:

(i) At the grid scale, the fraction of open water p or the ice thickness h could be defined not only from a mean value but also from higher order moments (such as the standard deviation) that would be explicitly introduced in the parametrization of variables like the ice strength P. Note however that the non-Gaussian character reported here implies that the mean and standard deviations are not sufficient to fully describe the spatial variability of p or $\mathrm{d}\varepsilon/\mathrm{d}t$. Instead the full set of moments is necessary. This is particularly true when looking at smaller and smaller scales, where the multifractal statistics imply a stronger and stronger departure from a Gaussian behavior (i.e., localisation/intermittency becomes more and more dominant).

(ii) Random multiplicative cascade models could de used to generate scale invariant fields to set the different moments of the grid values, taking into account the grid scale L (which can vary from cell to cell, see, e.g., Fichelet and Morales Maqueda [9]). This can be thought as a way to downscale the distribution from the climate models resolution scale to any (smaller) scale of particular interest.

(iii) The modelling of the feedbacks of the ice cover dynamics and fracturing on the fraction of open water should be improved, particularly in non-summer conditions when fracturing is particularly important. This should be done keeping in mind once again the problem of scaling, which implies that a mean is insufficient to describe the deformation field.

As a conclusion to this section, we stress that the scaling properties of sea ice deformation and fracturing raise numerous difficulties when homogenization is used to model complex, non-linear thermodynamic and mechanical processes. This opens new questions in the modelling of sea ice dynamics as well as air-ice-ocean interactions within climate models.

4.3. Constraints on sea ice dynamics models

Since the pioneering work of Hibler [10], various sea ice dynamics models have been developed. The sea ice modules of climate models are derived from simplified versions of these more specific, dynamical models. Most of these ice dynamics models are based on a continuum mechanics framework with a momentum balance given by Eq. (1), and share a common viscous-plastic rheology (Eq. (2)). One of the main challenges for these models is to reproduce the observed heterogeneity of deformation. In recent model developments, this is achieved through a weakening mechanism where the ice strength P is related to the divergence of the ice velocity $\nabla \cdot u$ following (Hutchings and Hibler [60]):

$$\frac{\mathrm{d}P}{\mathrm{d}t} \sim -P\nabla \cdot u. \tag{7}$$

This positive feedback loop (large deformation $\Rightarrow$ large weakening $\Rightarrow$ larger deformation), associated with some initial noise on the strength, generates localization of the deformation. This agreement with observations is, however, essentially qualitative and, to our opinion, not sufficient, and depends on the scale of discretization of the model. The results reported here furnish a detailed and quantitative characterization of the heterogeneity of sea ice deformation at all scales. The multifractality of sea ice deformation and fracturing, expressed by the moment functions, should therefore constrain further developments in sea ice dynamics modelling. A satisfying modelling should be able to generate scale invariant, multifractal deformation fields.

Finally, whether or not the viscous-plastic rheology used in these models is pertinent can be questioned. Indeed, as we stressed above, the multifractality of sea ice means that deformation becomes more localized towards small scales. Marsan et al. [54], extrapolated the pdf of $\mathrm{d}\varepsilon/\mathrm{d}t$ at the scale of 1 m (about the ice cover thickness) from the pdf at the scale of 13 km using the multifractal scaling that characterize the data. They showed that at this 1 m scale about 15% of the deformation was accommodated at strain-rates larger than 10^{-4} s^{-1}, i.e. in a purely brittle behaviour for saline ice (Schulson [12]). Moreover, these strain-rates were calculated for a three-day time scale. We have shown in Section 3.3 that ice stresses (so, the deformation) are intermittent at shorter time scales. This implies that this percentage should increase, meaning that most of the deformation could be accommodated through elasto-brittle deformation. The use of a plastic rheology instead of a elasto-brittle one can however be proposed as a way of accounting for the collective behaviour of a large set of fractures and leads that interact with each other, and with sizes smaller than the resolution scale, or equivalently as a particular case of an emerging rheology for a damaged elasto-brittle material (Amitrano et al. [61]).

Acknowledgements

We thank J. Richter-Menge and B. Elder who provided the stress records of the SHEBA experiment. Many discussions with Ron Lindsay, Harry Stern, Hubert Gallée and François Schmitt have helped improving this manuscript. This work was performed within the framework of a CNRS-NSF collaborative program.

References

[1] R.E. Moritz, C.M. Bitz, E.J. Steig, Dynamics of recent climate change in the Arctic, Science 297 (2002) 1497–1502.
[2] J. Zhang, D. Rothrock, M. Steele, Recent changes in arctic sea ice: the interplay between ice dynamics and thermodynamics, J. Climate 13 (17) (2000) 3099–3114.
[3] G.A. Maykut, Large scale heat exchange and ice production in the central Arctic, J. Geophys. Res. 87 (C10) (1982) 7971–7984.
[4] J. Morison, K. Aagaard, M. Steele, Recent environmental changes in the Arctic: a review, Arctic 53 (4) (2000) 359–371.
[5] R.A. Kerr, Will the Arctic Ocean lose all its ice?, Science 286 (1999) 1828.
[6] D.A. Rothrock, Y. Yu, G. Maykut, Thinning of the Arctic Sea Ice cover, Geophys. Res. Lett. 26 (23) (1999) 3469–3472.
[7] J.C. Comiso, A rapidly declining perennial sea ice cover in the Arctic, Geophys. Res. Lett. 29 (2002).
[8] R.A. Kerr, A warmer Arctic means change for all, Science 297 (2002) 1490–1492.
[9] T. Fichelet, M.A. Morales Maqueda, Sensitivity of a global sea ice model to the treatment of ice thermodynamics and dynamics, J. Geophys. Res. 102 (C6) (1997) 12609–12646.
[10] W.D.I. Hibler, A dynamic thermodynamics sea ice model, J. Phys. Oceanography 9 (1979) 815–846.
[11] D.M. Cole, The microstructure of ice and its influence on mechanical properties, Engrg. Fracture Mech. 68 (2001) 1797–1822.
[12] E.M. Schulson, Brittle failure of ice, Engrg. Fracture Mech. 68 (17/18) (2001) 1839–1887.

[13] C.A. Geiger, W.D.I. Hibler, S.F. Ackley, Large-scale sea ice drift and deformation: comparison between models and observations in the western Weddell Sea during 1992, J. Geophys. Res. 103 (C10) (1998) 21893–21913.
[14] J.K. Lewis, J.A. Richter-Menge, Motion-induced stresses in pack ice, J. Geophys. Res. 103 (C10) (1998) 21831–21843.
[15] S.L. McNutt, J.E. Overland, Spatial hierarchy in Arctic sea ice dynamics, Tellus 554 (2003) 181–191.
[16] J.E. Overland, B.A. Walter, T.B. Curtin, P. Turet, Hierarchy and Sea ice mechanics: a case study from the Beaufort Sea, J. Geophys. Res. 100 (C3) (1995) 4559–4571.
[17] E.M. Schulson, W.D. Hibler, The fracture of ice on scales large and small: Arctic leads and wing cracks, J. Glaciology 37 (1991) 319–322.
[18] M. Steele, J. Zhang, D. Rothrock, H. Stern, The force balance of sea ice in a numerical model of the Arctic Ocean, J. Geophys. Res. 102 (C9) (1997) 21061–21079.
[19] J.K. Lewis, Thermomechanics of pack ice, J. Geophys. Res. 103 (C10) (1998) 21869–21882.
[20] W.D.I. Hibler, Sea ice fracturing on the large scale, Engrg. Fracture Mech. 68 (2001) 2013–2043.
[21] R.W. Lindsay, H.L. Stern, A new Lagrangian model of arctic sea ice, J. Phys. Oceanography 34 (2004) 272–283.
[22] J.A. Richter-Menge, K.F. Jones, The tensile strength of first-year sea ice, J. Glaciology 39 (133) (1993) 609–618.
[23] H.E. Stanley, Scaling, universality, and renormalization: the three pillars of modern critical phenomena, Rev. Modern Phys. 71 (2) (1999) S358–S366.
[24] S. Lovejoy, D. Schertzer, Generalized scale invariance and fractal models of rain, Water Resources Res. 33 (1985) 2483–2488.
[25] C.J. Allègre, J.L. Le Mouel, A. Provost, Scaling rules in rock fracture and possible implications for earthquake prediction, Nature 297 (1982) 47–49.
[26] C.C. Barton, E. Larsen, Fractal geometry of 2-dimensional fracture networks at Yucca Mountain, southwestern Nevada, in: O. Stephanson (Ed.), International Symposium on Fundamentals of Rock Joints, Bjorkliden, 1985, pp. 77–84.
[27] W.L. Power, T.E. Tullis, S.R. Brown, G.N. Boitnott, C.H. Scholz, Roughness of natural fault surfaces, Geophys. Res. Lett. 14 (1) (1987) 29–32.
[28] I. Main, Statistical physics, seismogenesis, ans seismic hazard, Rev. Geophys. 34 (4) (1996) 433–462.
[29] E. Bonnet, O. Bour, N.E. Odling, P. Davy, I. Main, P. Cowie, B. Berkowitz, Scaling of fracture systems in geological media, Rev. Geophys. 39 (3) (2001) 347–383.
[30] B. Gutenberg, C.F. Richter, Seismicity of the Earth and Associated Phenomenon, Princeton University Press, Princeton, 1954.
[31] Y.Y. Kagan, D.D. Jackson, Long-term earthquake clustering, Geophys. J. Int. 104 (1991) 117–133.
[32] C. Kergomard, Analyse morphométrique de la zone marginale de la banquise polaire au nord-ouest du spitsberg à partir de l'imagerie SPOT panchromatique, Bull. SFPT 115 (1989) 17–20.
[33] R. Korsnes, S.R. Souza, R. Donangelo, A. Hansen, M. Paczuski, K. Sneppen, Scaling in fracture and refreezing of sea ice, Physica A 331 (2003) 291–296.
[34] M. Lensu, The fractality of sea ice cover, in: IAHR Ice Symposium, Espoo, Finland, 1990, pp. 300–313.
[35] M. Matsushita, Fractal viewpoint of fracture and accretion, J. Phys. Soc. Japan 54 (3) (1985) 857–860.
[36] D.A. Rothrock, A.S. Thorndike, Measuring the Sea Ice Floe Size Distribution, J. Geophys. Res. 89 (C4) (1984) 6477–6486.
[37] H.L. Stern, D.A. Rothrock, R. Kwok, Open water production in Arctic sea ice: satellite measurements and model parametrizations, J. Geophys. Res. 100 (C10) (1995) 20601–20612.
[38] J. Weiss, Scaling of fracture and faulting in ice on Earth, Surveys Geophys. 24 (2003) 185–227.
[39] G. Ouillon, C. Castaing, D. Sornette, Hierarchical geometry of faulting, J. Geophys. Res. 101 (B3) (1996) 5477–5487.
[40] J. Weiss, M. Gay, Fracturing of ice under compression creep as revealed by a multifractal analysis, J. Geophys. Res. 103 (B10) (1998) 24005–24016.
[41] D. Marsan, C.J. Bean, Multifractal modeling and analyses of crustal heterogeneity, in: J.A. Goff, K. Holliger (Eds.), Heterogeneity in the Crust and Upper Mantle, Kluwer Academic/Plenum Publishers, 2003, pp. 207–236.
[42] U. Frisch, Turbulence, The Legacy of A.N. Kolmogorov, Cambridge University Press, Cambridge, 1995.
[43] D. Schertzer, S. Lovejoy, F. Schmitt, Y. Chigirinskaia, D. Marsan, Multifractal cascade dynamics and turbulent intermittency, Fractals 5 (1997) 427–471.
[44] D. Schertzer, S. Lovejoy, Physical modeling and analysis of rain and clouds by anisotropic scaling multiplicative processes, J. Geophys. Res. 92 (D8) (1987) 9693–9714.
[45] F. Schmitt, D. Lavallée, D. Schertzer, S. Lovejoy, Empirical determination of universal multifractal exponents in turbulent velocity fields, Phys. Rev. Lett. 68 (1992) 305–308.
[46] F. Schmitt, S. Lovejoy, D. Schertzer, Multifractal analysis of the Greenland ice-core project climate data, Geophys. Res. Lett. 22 (13) (1995) 1689–1692.
[47] T. Falco, F. Francis, S. Lovejoy, D. Schertzer, B. Kerman, M. Drinkwater, Universal multifractal scaling of synthetic aperture radar images of sea-ice, IEEE Trans. Geosci. Remote Sensing 34 (4) (1996) 906–914.
[48] S. Martin, A.S. Thorndike, Dispersion of sea ice in the Bering Sea, J. Geophys. Res. 90 (C4) (1985) 7223–7226.
[49] G.I. Taylor, Diffusion by continuous movements, Proc. London Math. Soc. 20 (1920) 196–212.
[50] L.F. Richardson, Atmospheric diffusion shown on a distance-neighbour graph, Proc. Roy. Soc. London A 110 (1926) 709–737.
[51] M. Fily, D.A. Rothrock, Opening and closing of sea ice leads: digital measurements from synthetic aperture radar, J. Geophys. Res. 95 (C1) (1990) 789–796.
[52] R. Kwok, The RADARSAT geophysical processor system, in: C. Tsatsoulis, R. Kwok (Eds.), Analysis of SAR Data of the Polar Oceans, Springer-Verlag, 1998, pp. 235–257.
[53] R. Kwok, J. Curlander, R. McConnell, S. Pang, An ice motion tracking system at the Alaska SAR facility, IEEE J. Oceanic Engrg. 15 (1) (1990).

[54] D. Marsan, H. Stern, R. Lindsay, J. Weiss, Scale dependence and localization of the deformation of arctic sea ice, Phys. Rev. Lett. (2004), in press.
[55] Y.V. Dudko, H. Schmidt, K. von der Heydt, E.K. Scheer, Edge wave observation using remote seismoacoustic sensing of ice events in the Arctic, J. Geophys. Res. 103 (C10) (1998) 21775–21781.
[56] J.A. Richter-Menge, B.C. Elder, Characteristics of pack ice stress in the Alaskan Beaufort Sea, J. Geophys. Res. 103 (C10) (1998) 21817–21829.
[57] B. Mandelbrot, J. Van Ness, Fractional Brownian motions, fractional noises and applications, SIAM Rev. 10 (4) (1968) 422–437.
[58] P.A. Cowie, D. Sornette, C. Vanneste, Multifractal scaling properties of a growing fault population, Geophys. J. Int. 122 (1995) 457–469.
[59] H. Gallée, Air-sea interactions over Terra Nova Bay during winter: simulation with a coupled atmosphere-polynya model, J. Geophys. Res. 102 (D12) (1997) 13835–13849.
[60] J.K. Hutchings, W.D.I. Hibler, Modelling sea ice deformation with a viscous-plastic isotropic rheology, in: 16th IAHR International Symposium on Ice, Dunedin, New Zeland, 2002, pp. 59–67.
[61] D. Amitrano, J.R. Grasso, D. Hantz, From diffuse to localized damage through elastic interaction, Geophys. Res. Lett. 26 (14) (1999) 2109–2112.